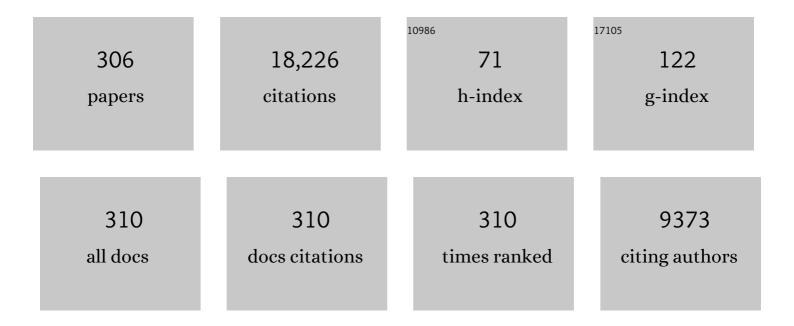
## List of Publications by Year in descending order

Source: https://exaly.com/author-pdf/1139060/publications.pdf Version: 2024-02-01



#	Article	IF	CITATIONS
1	Long-Term Results of the M. D. Anderson Randomized Dose-Escalation Trial for Prostate Cancer. International Journal of Radiation Oncology Biology Physics, 2008, 70, 67-74.	0.8	1,137
2	Quantification of volumetric and geometric changes occurring during fractionated radiotherapy for head-and-neck cancer using an integrated CT/linear accelerator system. International Journal of Radiation Oncology Biology Physics, 2004, 59, 960-970.	0.8	643
3	Validation of an accelerated â€~demons' algorithm for deformable image registration in radiation therapy. Physics in Medicine and Biology, 2005, 50, 2887-2905.	3.0	537
4	Increased risk of biochemical and local failure in patients with distended rectum on the planning CT for prostate cancer radiotherapy. International Journal of Radiation Oncology Biology Physics, 2005, 62, 965-973.	0.8	385
5	Dosimetry tools and techniques for IMRT. Medical Physics, 2011, 38, 1313-1338.	3.0	359
6	Assessing Respiration-Induced Tumor Motion and Internal Target Volume Using Four-Dimensional Computed Tomography for Radiotherapy of Lung Cancer. International Journal of Radiation Oncology Biology Physics, 2007, 68, 531-540.	0.8	306
7	Late rectal toxicity: dose-volume effects of conformal radiotherapy for prostate cancer. International Journal of Radiation Oncology Biology Physics, 2002, 54, 1314-1321.	0.8	279
8	Comprehensive analysis of proton range uncertainties related to patient stopping-power-ratio estimation using the stoichiometric calibration. Physics in Medicine and Biology, 2012, 57, 4095-4115.	3.0	273
9	Stereotactic Body Radiation Therapy in Centrally and Superiorly Located Stage I or Isolated Recurrent Non–Small-Cell Lung Cancer. International Journal of Radiation Oncology Biology Physics, 2008, 72, 967-971.	0.8	251
10	Quality assurance for imageâ€guided radiation therapy utilizing CTâ€based technologies: A report of the AAPM TGâ€179. Medical Physics, 2012, 39, 1946-1963.	3.0	251
11	Use of deformed intensity distributions for on-line modification of image-guided IMRT to account for interfractional anatomic changes. International Journal of Radiation Oncology Biology Physics, 2005, 61, 1258-1266.	0.8	218
12	Beat frequency quartz-enhanced photoacoustic spectroscopy for fast and calibration-free continuous trace-gas monitoring. Nature Communications, 2017, 8, 15331.	12.8	213
13	An evidence based review of proton beam therapy: The report of ASTRO's emerging technology committee. Radiotherapy and Oncology, 2012, 103, 8-11.	0.6	212
14	Reducing metal artifacts in cone-beam CT images by preprocessing projection data. International Journal of Radiation Oncology Biology Physics, 2007, 67, 924-932.	0.8	209
15	Osteoradionecrosis and Radiation Dose to the Mandible in Patients With Oropharyngeal Cancer. International Journal of Radiation Oncology Biology Physics, 2013, 85, 415-420.	0.8	209
16	Adaptive Radiotherapy for Head-and-Neck Cancer: Initial Clinical Outcomes From a Prospective Trial. International Journal of Radiation Oncology Biology Physics, 2012, 83, 986-993.	0.8	205
17	Feasibility of sparing lung and other thoracic structures with intensity-modulated radiotherapy for non–small-cell lung cancer. International Journal of Radiation Oncology Biology Physics, 2004, 58, 1268-1279.	0.8	199
18	Intrafraction prostate motion during IMRT for prostate cancer. International Journal of Radiation Oncology Biology Physics, 2002, 53, 261-268.	0.8	193

#	Article	IF	CITATIONS
19	Report of the <scp>AAPM TG</scp> â€256 on the relative biological effectiveness of proton beams in radiation therapy. Medical Physics, 2019, 46, e53-e78.	3.0	189
20	4D Proton treatment planning strategy for mobile lung tumors. International Journal of Radiation Oncology Biology Physics, 2007, 67, 906-914.	0.8	178
21	Recent advances in quartz enhanced photoacoustic sensing. Applied Physics Reviews, 2018, 5, .	11.3	174
22	Implementation and validation of a three-dimensional deformable registration algorithm for targeted prostate cancer radiotherapy. International Journal of Radiation Oncology Biology Physics, 2005, 61, 725-735.	0.8	168
23	Adaptive radiotherapy for head and neck cancer—Dosimetric results from a prospective clinical trial. Radiotherapy and Oncology, 2013, 106, 80-84.	0.6	168
24	Multiple regions-of-interest analysis of setup uncertainties for head-and-neck cancer radiotherapy. International Journal of Radiation Oncology Biology Physics, 2006, 64, 1559-1569.	0.8	165
25	Consensus Guidelines for Implementing Pencil-Beam Scanning Proton Therapy for Thoracic Malignancies on Behalf of the PTCOG Thoracic and Lymphoma Subcommittee. International Journal of Radiation Oncology Biology Physics, 2017, 99, 41-50.	0.8	162
26	Candidate Dosimetric Predictors of Long-Term Swallowing Dysfunction After Oropharyngeal Intensity-Modulated Radiotherapy. International Journal of Radiation Oncology Biology Physics, 2010, 78, 1356-1365.	0.8	156
27	Compact TDLAS based sensor design using interband cascade lasers for mid-IR trace gas sensing. Optics Express, 2016, 24, A528.	3.4	150
28	A Beam-Specific Planning Target Volume (PTV) Design for Proton Therapy to Account for Setup and Range Uncertainties. International Journal of Radiation Oncology Biology Physics, 2012, 82, e329-e336.	0.8	145
29	Experience of ultrasound-based daily prostate localization. International Journal of Radiation Oncology Biology Physics, 2003, 56, 436-447.	0.8	144
30	Effectiveness of robust optimization in intensityâ€modulated proton therapy planning for head and neck cancers. Medical Physics, 2013, 40, 051711.	3.0	135
31	Objective assessment of deformable image registration in radiotherapy: A multiâ€institution study. Medical Physics, 2008, 35, 5944-5953.	3.0	132
32	Disease-control rates following intensity-modulated radiation therapy for small primary oropharyngeal carcinoma. International Journal of Radiation Oncology Biology Physics, 2007, 67, 438-444.	0.8	130
33	Parotid Gland Dose in Intensity-Modulated Radiotherapy for Head and Neck Cancer: Is What You Plan What You Get?. International Journal of Radiation Oncology Biology Physics, 2007, 69, 1290-1296.	0.8	130
34	Quartz enhanced photoacoustic H2S gas sensor based on a fiber-amplifier source and a custom tuning fork with large prong spacing. Applied Physics Letters, 2015, 107, .	3.3	128
35	Investigation of bladder dose and volume factors influencing late urinary toxicity after external beam radiotherapy for prostate cancer. International Journal of Radiation Oncology Biology Physics, 2007, 67, 1059-1065.	0.8	127
36	Physics Controversies in Proton Therapy. Seminars in Radiation Oncology, 2013, 23, 88-96.	2.2	127

#	Article	IF	CITATIONS
37	Atmospheric CH4 measurement near a landfill using an ICL-based QEPAS sensor with V-T relaxation self-calibration. Sensors and Actuators B: Chemical, 2019, 297, 126753.	7.8	127
38	An automatic CT-guided adaptive radiation therapy technique by online modification of multileaf collimator leaf positions for prostate cancer. International Journal of Radiation Oncology Biology Physics, 2005, 62, 154-163.	0.8	125
39	Ppb-level detection of nitric oxide using an external cavity quantum cascade laser based QEPAS sensor. Optics Express, 2011, 19, 24037.	3.4	122
40	Intensity-Modulated Proton Therapy Further Reduces Normal Tissue Exposure During Definitive Therapy for Locally Advanced Distal Esophageal Tumors: A Dosimetric Study. International Journal of Radiation Oncology Biology Physics, 2011, 81, 1336-1342.	0.8	122
41	Hazards of dose escalation in prostate cancer radiotherapy. International Journal of Radiation Oncology Biology Physics, 2003, 57, 1260-1268.	0.8	121
42	Image Guided Radiation Therapy (IGRT) Technologies for Radiation Therapy Localization and Delivery. International Journal of Radiation Oncology Biology Physics, 2013, 87, 33-45.	0.8	120
43	Effectiveness of noncoplanar IMRT planning using a parallelized multiresolution beam angle optimization method for paranasal sinus carcinoma. International Journal of Radiation Oncology Biology Physics, 2005, 63, 594-601.	0.8	119
44	Reduce in Variation and Improve Efficiency of Target Volume Delineation by a Computer-Assisted System Using a Deformable Image Registration Approach. International Journal of Radiation Oncology Biology Physics, 2007, 68, 1512-1521.	0.8	113
45	Comparison of 2D Radiographic Images and 3D Cone Beam Computed Tomography for Positioning Head-and-Neck Radiotherapy Patients. International Journal of Radiation Oncology Biology Physics, 2008, 71, 916-925.	0.8	112
46	Intensity-modulated radiotherapy following extrapleural pneumonectomy for the treatment of malignant mesothelioma: clinical implementation. International Journal of Radiation Oncology Biology Physics, 2003, 55, 606-616.	0.8	110
47	Compact TDLAS based optical sensor for ppb-level ethane detection by use of a 3.34 μm room-temperature CW interband cascade laser. Sensors and Actuators B: Chemical, 2016, 232, 188-194.	7.8	108
48	Evaluation of mechanical precision and alignment uncertainties for an integrated CT/LINAC system. Medical Physics, 2003, 30, 1198-1210.	3.0	107
49	Automatic Segmentation of Whole Breast Using Atlas Approach and Deformable Image Registration. International Journal of Radiation Oncology Biology Physics, 2009, 73, 1493-1500.	0.8	102
50	Use of portal images and BAT ultrasonography to measure setup error and organ motion for prostate IMRT: implications for treatment margins. International Journal of Radiation Oncology Biology Physics, 2003, 56, 1218-1224.	0.8	101
51	Image–Guided Radiation Therapy for Non–small Cell Lung Cancer. Journal of Thoracic Oncology, 2008, 3, 177-186.	1.1	101
52	Compact CH4 sensor system based on a continuous-wave, low power consumption, room temperature interband cascade laser. Applied Physics Letters, 2016, 108, .	3.3	101
53	Patient-specific point dose measurement for IMRT monitor unit verification. International Journal of Radiation Oncology Biology Physics, 2003, 56, 867-877.	0.8	100
54	Patterns of Disease Recurrence Following Treatment of Oropharyngeal Cancer With Intensity Modulated Radiation Therapy. International Journal of Radiation Oncology Biology Physics, 2013, 85, 941-947.	0.8	99

#	Article	IF	CITATIONS
55	Performance Evaluation of Automatic Anatomy Segmentation Algorithm on Repeat or Four-Dimensional Computed Tomography Images Using Deformable Image Registration Method. International Journal of Radiation Oncology Biology Physics, 2008, 72, 210-219.	0.8	98
56	Automatic registration of the prostate for computed-tomography-guided radiotherapy. Medical Physics, 2003, 30, 2750-2757.	3.0	94
57	Comparison of rectal dose–wall histogram versus dose–volume histogram for modeling the incidence of late rectal bleeding after radiotherapy. International Journal of Radiation Oncology Biology Physics, 2004, 60, 1589-1601.	0.8	94
58	Enhanced near-infrared QEPAS sensor for sub-ppm level H2S detection by means of a fiber amplified 1582 nm DFB laser. Sensors and Actuators B: Chemical, 2015, 221, 666-672.	7.8	91
59	Sub-ppb nitrogen dioxide detection with a large linear dynamic range by use of a differential photoacoustic cell and a 3.5 W blue multimode diode laser. Sensors and Actuators B: Chemical, 2017, 247, 329-335.	7.8	90
60	Effect of anatomic motion on proton therapy dose distributions in prostate cancer treatment. International Journal of Radiation Oncology Biology Physics, 2007, 67, 620-629.	0.8	89
61	Single-tube on-beam quartz-enhanced photoacoustic spectroscopy. Optics Letters, 2016, 41, 978.	3.3	88
62	Monte Carlo simulations of the dosimetric impact of radiopaque fiducial markers for proton radiotherapy of the prostate. Physics in Medicine and Biology, 2007, 52, 2937-2952.	3.0	83
63	Proton Radiotherapy for Liver Tumors: Dosimetric Advantages Over Photon Plans. Medical Dosimetry, 2008, 33, 259-267.	0.9	83
64	Clinical Practice Guidance for Radiotherapy Planning After Induction Chemotherapy in Locoregionally Advanced Head-and-Neck Cancer. International Journal of Radiation Oncology Biology Physics, 2009, 75, 725-733.	0.8	80
65	Intensity modulated radiation therapy (IMRT) following prostatectomy: more favorable acute genitourinary toxicity profile compared to primary IMRT for prostate cancer. International Journal of Radiation Oncology Biology Physics, 2001, 49, 465-472.	0.8	79
66	ppb-Level SO <sub>2</sub> Photoacoustic Sensors with a Suppressed Absorption–Desorption Effect by Using a 7.41 μm External-Cavity Quantum Cascade Laser. ACS Sensors, 2020, 5, 549-556.	7.8	79
67	Quartz-enhanced photoacoustic spectroscopy for multi-gas detection: A review. Analytica Chimica Acta, 2022, 1202, 338894.	5.4	79
68	Estimation of $\hat{I} \pm / \hat{I}^2$ for Late Rectal Toxicity Based on RTOG 94-06. International Journal of Radiation Oncology Biology Physics, 2011, 81, 600-605.	0.8	76
69	High and flat spectral responsivity of quartz tuning fork used as infrared photodetector in tunable diode laser spectroscopy. Applied Physics Reviews, 2021, 8, .	11.3	76
70	The Use of Rectal Balloon During the Delivery of Intensity Modulated Radiotherapy (IMRT) for Prostate Cancer. Cancer Journal (Sudbury, Mass ), 2002, 8, 476-483.	2.0	75
71	Impact of respiratory motion on worst-case scenario optimized intensity modulated proton therapy for lung cancers. Practical Radiation Oncology, 2015, 5, e77-e86.	2.1	75
72	Development of methods for beam angle optimization for IMRT using an accelerated exhaustive search strategy. International Journal of Radiation Oncology Biology Physics, 2004, 60, 1325-1337.	0.8	74

#	Article	IF	CITATIONS
73	Quantification of Prostate and Seminal Vesicle Interfraction Variation During IMRT. International Journal of Radiation Oncology Biology Physics, 2008, 71, 813-820.	0.8	74
74	Mid-infrared dual-gas sensor for simultaneous detection of methane and ethane using a single continuous-wave interband cascade laser. Optics Express, 2016, 24, 16973.	3.4	74
75	Evaluation of respiratory-induced target motion for esophageal tumors at the gastroesophageal junction. Radiotherapy and Oncology, 2007, 84, 283-289.	0.6	73
76	Trace gas detection based on off-beam quartz enhanced photoacoustic spectroscopy: Optimization and performance evaluation. Review of Scientific Instruments, 2010, 81, 103103.	1.3	70
77	Ppb-level QEPAS NO2 sensor by use of electrical modulation cancellation method with a high power blue LED. Sensors and Actuators B: Chemical, 2015, 208, 173-179.	7.8	70
78	An image correlation procedure for digitally reconstructed radiographs and electronic portal images. International Journal of Radiation Oncology Biology Physics, 1995, 33, 1053-1060.	0.8	69
79	Dose–response characteristics of low- and intermediate-risk prostate cancer treated with external beam radiotherapy. International Journal of Radiation Oncology Biology Physics, 2005, 61, 993-1002.	0.8	68
80	Dose Constraints to Prevent Radiation-Induced Brachial Plexopathy in Patients Treated for Lung Cancer. International Journal of Radiation Oncology Biology Physics, 2012, 82, e391-e398.	0.8	67
81	Ppb-Level Quartz-Enhanced Photoacoustic Detection of Carbon Monoxide Exploiting a Surface Grooved Tuning Fork. Analytical Chemistry, 2019, 91, 5834-5840.	6.5	67
82	Three-Dimensional Printed Miniature Fiber-Coupled Multipass Cells with Dense Spot Patterns for ppb-Level Methane Detection Using a Near-IR Diode Laser. Analytical Chemistry, 2020, 92, 13034-13041.	6.5	67
83	Dose–volume response analyses of late rectal bleeding after radiotherapy for prostate cancer. International Journal of Radiation Oncology Biology Physics, 2004, 59, 353-365.	0.8	66
84	Rapid radiographic film calibration for IMRT verification using automated MLC fields. Medical Physics, 2002, 29, 2384-2390.	3.0	64
85	Simultaneous dual-gas QEPAS detection based on a fundamental and overtone combined vibration of quartz tuning fork. Applied Physics Letters, 2017, 110, .	3.3	64
86	Compact photoacoustic module for methane detection incorporating interband cascade light emitting device. Optics Express, 2017, 25, 16761.	3.4	63
87	Ppb-level photoacoustic sensor system for saturation-free CO detection of SF6 decomposition by use of a 10 W fiber-amplified near-infrared diode laser. Sensors and Actuators B: Chemical, 2019, 282, 567-573.	7.8	63
88	Ultrasound-Based Localization. Seminars in Radiation Oncology, 2005, 15, 180-191.	2.2	62
89	Dosimetric accuracy of Kodak EDR2 film for IMRT verifications. Medical Physics, 2005, 32, 539-548.	3.0	61
90	A deformable image registration method to handle distended rectums in prostate cancer radiotherapy. Medical Physics, 2006, 33, 3304-3312.	3.0	61

#	Article	IF	CITATIONS
91	Development and field deployment of a mid-infrared methane sensor without pressure control using interband cascade laser absorption spectroscopy. Sensors and Actuators B: Chemical, 2017, 244, 365-372.	7.8	61
92	Accuracy of two heterogeneity dose calculation algorithms for IMRT in treatment plans designed using an anthropomorphic thorax phantom. Medical Physics, 2007, 34, 1850-1857.	3.0	60
93	Late Rectal Toxicity on RTOG 94-06: Analysis Using a Mixture Lyman Model. International Journal of Radiation Oncology Biology Physics, 2010, 78, 1253-1260.	0.8	60
94	Double acoustic microresonator quartz-enhanced photoacoustic spectroscopy. Optics Letters, 2014, 39, 2479.	3.3	58
95	Ppb-level formaldehyde detection using a CW room-temperature interband cascade laser and a miniature dense pattern multipass gas cell. Optics Express, 2015, 23, 19821.	3.4	58
96	Analysis of overtone flexural modes operation in quartz-enhanced photoacoustic spectroscopy. Optics Express, 2016, 24, A682.	3.4	57
97	Ppb-level gas detection using on-beam quartz-enhanced photoacoustic spectroscopy based on a 28ÂkHz tuning fork. Photoacoustics, 2022, 25, 100321.	7.8	57
98	Characterization of rectal normal tissue complication probability after high-dose external beam radiotherapy for prostate cancer. International Journal of Radiation Oncology Biology Physics, 2004, 58, 1513-1519.	0.8	56
99	Adaptive Radiation Therapy for Head and Neck Cancer—Can an Old Goal Evolve into a New Standard?. Journal of Oncology, 2011, 2011, 1-13.	1.3	56
100	Dosimetric benefits of robust treatment planning for intensity modulated proton therapy for base-of-skull cancers. Practical Radiation Oncology, 2014, 4, 384-391.	2.1	56
101	Rectal wall sparing by dosimetric effect of rectal balloon used during Intensity-Modulated Radiation Therapy (IMRT) for prostate cancer. Medical Dosimetry, 2005, 30, 25-30.	0.9	55
102	Beam angle optimization and reduction for intensity-modulated radiation therapy of non–small-cell lung cancers. International Journal of Radiation Oncology Biology Physics, 2006, 65, 561-572.	0.8	55
103	Speed and convergence properties of gradient algorithms for optimization of IMRT. Medical Physics, 2004, 31, 1141-1152.	3.0	53
104	Statistical Assessment of Proton Treatment Plans Under Setup and Range Uncertainties. International Journal of Radiation Oncology Biology Physics, 2013, 86, 1007-1013.	0.8	53
105	Dual-Gas Quartz-Enhanced Photoacoustic Sensor for Simultaneous Detection of Methane/Nitrous Oxide and Water Vapor. Analytical Chemistry, 2019, 91, 12866-12873.	6.5	53
106	Highly sensitive and selective CO sensor using a 233 μm diode laser and wavelength modulation spectroscopy. Optics Express, 2018, 26, 24318.	3.4	52
107	Light-induced thermo-elastic effect in quartz tuning forks exploited as a photodetector in gas absorption spectroscopy. Optics Express, 2020, 28, 19074.	3.4	51
108	Evaluation of a contour-alignment technique for CT-guided prostate radiotherapy: an intra- and interobserver study. International Journal of Radiation Oncology Biology Physics, 2004, 59, 412-418.	0.8	50

#	Article	IF	CITATIONS
109	Dosimetric comparison of four target alignment methods for prostate cancer radiotherapy. International Journal of Radiation Oncology Biology Physics, 2006, 66, 883-891.	0.8	49
110	Impact of Humidity on Quartz-Enhanced Photoacoustic Spectroscopy Based CO Detection Using a Near-IR Telecommunication Diode Laser. Sensors, 2016, 16, 162.	3.8	49
111	Highly sensitive SO_2 photoacoustic sensor for SF_6 decomposition detection using a compact mW-level diode-pumped solid-state laser emitting at 303 nm. Optics Express, 2017, 25, 32581.	3.4	49
112	Highly sensitive photoacoustic multicomponent gas sensor for SF <sub>6</sub> decomposition online monitoring. Optics Express, 2019, 27, A224.	3.4	49
113	Ppb-level H2S detection for SF6 decomposition based on a fiber-amplified telecommunication diode laser and a background-gas-induced high- <i>Q</i> photoacoustic cell. Applied Physics Letters, 2017, 111,	3.3	48
114	Cluster model analysis of late rectal bleeding after IMRT of prostate cancer: A case–control study. International Journal of Radiation Oncology Biology Physics, 2006, 64, 1255-1264.	0.8	47
115	Modeling respiratory motion for reducing motion artifacts in 4D CT images. Medical Physics, 2013, 40, 041716.	3.0	47
116	Broadband detection of methane and nitrous oxide using a distributed-feedback quantum cascade laser array and quartz-enhanced photoacoustic sensing. Photoacoustics, 2020, 17, 100159.	7.8	47
117	Development of a coal quality analyzer for application to power plants based on laser-induced breakdown spectroscopy. Spectrochimica Acta, Part B: Atomic Spectroscopy, 2015, 113, 167-173.	2.9	46
118	Overtone resonance enhanced single-tube on-beam quartz enhanced photoacoustic spectrophone. Applied Physics Letters, 2016, 109, .	3.3	46
119	Development and performance evaluation of self-absorption-free laser-induced breakdown spectroscopy for directly capturing optically thin spectral line and realizing accurate chemical composition measurements. Optics Express, 2017, 25, 23024.	3.4	46
120	Quartz-enhanced photoacoustic sensor for ethylene detection implementing optimized custom tuning fork-based spectrophone. Optics Express, 2019, 27, 4271.	3.4	46
121	Integrated beam orientation and scanningâ€spot optimization in intensityâ€modulated proton therapy for brain and unilateral head and neck tumors. Medical Physics, 2018, 45, 1338-1350.	3.0	45
122	A method of simulating dynamic multileaf collimators using Monte Carlo techniques for intensity-modulated radiation therapy. Physics in Medicine and Biology, 2001, 46, 2283-2298.	3.0	44
123	Toward a better understanding of the gamma index: Investigation of parameters with a surfaceâ€based	3.0	44
124	Recent progress on laser-induced breakdown spectroscopy for the monitoring of coal quality and unburned carbon in fly ash. Frontiers of Physics, 2012, 7, 690-700.	5.0	44
125	Quartz–enhanced photoacoustic spectrophones exploiting custom tuning forks: a review. Advances in Physics: X, 2017, 2, 169-187.	4.1	44
126	Quartz-enhanced photoacoustic spectroscopy for hydrocarbon trace gas detection and petroleum exploration. Fuel, 2020, 277, 118118.	6.4	43

#	Article	IF	CITATIONS
127	Quartz-enhanced photoacoustic spectroscopy exploiting low-frequency tuning forks as a tool to measure the vibrational relaxation rate in gas species. Photoacoustics, 2021, 21, 100227.	7.8	43
128	Partial Least-Squares Regression as a Tool to Retrieve Gas Concentrations in Mixtures Detected Using Quartz-Enhanced Photoacoustic Spectroscopy. Analytical Chemistry, 2020, 92, 11035-11043.	6.5	42
129	Mid-Infrared Quartz-Enhanced Photoacoustic Sensor for ppb-Level CO Detection in a SF <sub>6</sub> Gas Matrix Exploiting a T-Grooved Quartz Tuning Fork. Analytical Chemistry, 2020, 92, 13922-13929.	6.5	42
130	Comparison of multiâ€institutional Varian ProBeam pencil beam scanning proton beam commissioning data. Journal of Applied Clinical Medical Physics, 2017, 18, 96-107.	1.9	42
131	Calculation model of dense spot pattern multi-pass cells based on a spherical mirror aberration. Optics Letters, 2019, 44, 1108.	3.3	42
132	Changes in the Pelvic Anatomy After an IMRT Treatment Fraction of Prostate Cancer. International Journal of Radiation Oncology Biology Physics, 2007, 68, 1529-1536.	0.8	41
133	High-concentration methane and ethane QEPAS detection employing partial least squares regression to filter out energy relaxation dependence on gas matrix composition. Photoacoustics, 2022, 26, 100349.	7.8	41
134	Dose sculpting with generalized equivalent uniform dose. Medical Physics, 2005, 32, 1387-1396.	3.0	40
135	Dose-response for biochemical control among high-risk prostate cancer patients after external beam radiotherapy. International Journal of Radiation Oncology Biology Physics, 2003, 56, 1234-1240.	0.8	39
136	A comparison of tumor motion characteristics between early stage and locally advanced stage lung cancers. Radiotherapy and Oncology, 2012, 104, 33-38.	0.6	39
137	Verification of radiosurgery target point alignment with an electronic portal imaging device (EPID). Medical Physics, 1997, 24, 263-267.	3.0	38
138	Quality of Life and Toxicity From Passively Scattered and Spot-Scanning Proton Beam Therapy for Localized Prostate Cancer. International Journal of Radiation Oncology Biology Physics, 2013, 87, 946-953.	0.8	38
139	Fiber-Amplifier-Enhanced QEPAS Sensor for Simultaneous Trace Gas Detection of NH3 and H2S. Sensors, 2015, 15, 26743-26755.	3.8	38
140	Calibration-free mid-infrared exhaled breath sensor based on BF-QEPAS for real-time ammonia measurements at ppb level. Sensors and Actuators B: Chemical, 2022, 358, 131510.	7.8	38
141	A portal image alignment and patient setup verification procedure using moments and correlation techniques. Physics in Medicine and Biology, 1996, 41, 697-723.	3.0	37
142	Automatic contouring of brachial plexus using a multi-atlas approach for lung cancer radiation therapy. Practical Radiation Oncology, 2013, 3, e139-e147.	2.1	37
143	H2S quartz-enhanced photoacoustic spectroscopy sensor employing a liquid-nitrogen-cooled THz quantum cascade laser operating in pulsed mode. Photoacoustics, 2021, 21, 100219.	7.8	37
144	Lack of Correlation Between External Fiducial Positions and Internal Tumor Positions During Breath-Hold CT. International Journal of Radiation Oncology Biology Physics, 2010, 76, 1586-1591.	0.8	36

#	Article	IF	CITATIONS
145	Position effects of acoustic micro-resonator in quartz enhanced photoacoustic spectroscopy. Sensors and Actuators B: Chemical, 2015, 206, 364-370.	7.8	36
146	ls a 3-mm intrafractional margin sufficient for daily image-guided intensity-modulated radiation therapy of prostate cancer?. Radiotherapy and Oncology, 2007, 85, 251-259.	0.6	35
147	Advantages of simulating thoracic cancer patients in an upright position. Practical Radiation Oncology, 2014, 4, e53-e58.	2.1	35
148	Retrospective analysis of 2D patient-specific IMRT verifications. Medical Physics, 2005, 32, 838-850.	3.0	34
149	Elastic image mapping for 4-D dose estimation in thoracic radiotherapy. Radiation Protection Dosimetry, 2005, 115, 497-502.	0.8	34
150	Assessment of shoulder position variation and its impact on IMRT and VMAT doses for head and neck cancer. Radiation Oncology, 2012, 7, 19.	2.7	34
151	Infrared Dual-Gas CH <sub>4</sub> /C <sub>2</sub> H <sub>6</sub> Sensor Using Two Continuous-Wave Interband Cascade Lasers. IEEE Photonics Technology Letters, 2016, 28, 2351-2354.	2.5	34
152	Compact and Highly Sensitive NO2 Photoacoustic Sensor for Environmental Monitoring. Molecules, 2020, 25, 1201.	3.8	34
153	The Effect of Dental Artifacts, Contrast Media, and Experience on Interobserver Contouring Variations in Head and Neck Anatomy. American Journal of Clinical Oncology: Cancer Clinical Trials, 2007, 30, 191-198.	1.3	33
154	Effectiveness of Using Fewer Implanted Fiducial Markers for Prostate Target Alignment. International Journal of Radiation Oncology Biology Physics, 2009, 74, 1283-1289.	0.8	33
155	Anatomic Distribution of Fluorodeoxyglucose-Avid Para-aortic Lymph Nodes in Patients With Cervical Cancer. International Journal of Radiation Oncology Biology Physics, 2013, 85, 1045-1050.	0.8	33
156	Double antinode excited quartz-enhanced photoacoustic spectrophone. Applied Physics Letters, 2017, 110, .	3.3	33
157	Palm-sized methane TDLAS sensor based on a mini-multi-pass cell and a quartz tuning fork as a thermal detector. Optics Express, 2021, 29, 12357.	3.4	33
158	Compact QEPAS humidity sensor in SF6 buffer gas for high-voltage gas power systems. Photoacoustics, 2022, 25, 100319.	7.8	33
159	Quantifying the Interfractional Displacement of the Gastroesophageal Junction During Radiation Therapy for Esophageal Cancer. International Journal of Radiation Oncology Biology Physics, 2012, 83, e273-e280.	0.8	31
160	Efficiency of respiratory-gated delivery of synchrotron-based pulsed proton irradiation. Physics in Medicine and Biology, 2008, 53, 1947-1959.	3.0	30
161	Current clinical coverage of Radiation Therapy Oncology Group-defined target volumes for postmastectomy radiation therapy. Practical Radiation Oncology, 2012, 2, 201-209.	2.1	30
162	A sixâ€year review of more than 13,000 patientâ€specific IMRT QA results from 13 different treatment sites. Journal of Applied Clinical Medical Physics, 2014, 15, 196-206.	1.9	30

#	Article	IF	CITATIONS
163	Application of acoustic micro-resonators in quartz-enhanced photoacoustic spectroscopy for trace gas analysis. Chemical Physics Letters, 2018, 691, 462-472.	2.6	30
164	Ppb-level nitric oxide photoacoustic sensor based on a mid-IR quantum cascade laser operating at 52 °C. Sensors and Actuators B: Chemical, 2019, 290, 426-433.	7.8	30
165	Auto-segmentation of low-risk clinical target volume for head and neck radiation therapy. Practical Radiation Oncology, 2014, 4, e31-e37.	2.1	28
166	Scattered light modulation cancellation method for sub-ppb-level NO_2 detection in a LD-excited QEPAS system. Optics Express, 2016, 24, A752.	3.4	28
167	Robust beam orientation optimization for intensityâ€modulated proton therapy. Medical Physics, 2019, 46, 3356-3370.	3.0	28
168	Dosimetric Performance and Planning/Delivery Efficiency of a Dual-Layer Stacked and Staggered MLC on Treating Multiple Small Targets: A Planning Study Based on Single-Isocenter Multi-Target Stereotactic Radiosurgery (SRS) to Brain Metastases. Frontiers in Oncology, 2019, 9, 7.	2.8	28
169	Cluster models of dose–volume effects. International Journal of Radiation Oncology Biology Physics, 2004, 59, 1491-1504.	0.8	26
170	Comparison of Treatment Volumes and Techniques in Prostate Cancer Radiation Therapy. American Journal of Clinical Oncology: Cancer Clinical Trials, 2005, 28, 618-625.	1.3	26
171	Tumor-Volume Simulation During Radiotherapy for Head-and-Neck Cancer Using a Four-Level Cell Population Model. International Journal of Radiation Oncology Biology Physics, 2009, 75, 595-602.	0.8	26
172	Do Intermediate Radiation Doses Contribute to Late Rectal Toxicity? An Analysis of Data From Radiation Therapy Oncology Group Protocol 94-06. International Journal of Radiation Oncology Biology Physics, 2012, 84, 390-395.	0.8	26
173	Acoustic Coupling between Resonator Tubes in Quartz-Enhanced Photoacoustic Spectrophones Employing a Large Prong Spacing Tuning Fork. Sensors, 2019, 19, 4109.	3.8	26
174	Daily Alignment Results of In-Room Computed Tomography–Guided Stereotactic Body Radiation Therapy for Lung Cancer. International Journal of Radiation Oncology Biology Physics, 2011, 79, 473-480.	0.8	25
175	Quartz-enhanced photoacoustic NH3 sensor exploiting a large-prong-spacing quartz tuning fork and an optical fiber amplifier for biomedical applications. Photoacoustics, 2022, 26, 100363.	7.8	25
176	Evaluation of Tumor Position and PTV Margins Using Image Guidance and Respiratory Gating. International Journal of Radiation Oncology Biology Physics, 2010, 76, 1578-1585.	0.8	24
177	Calibration-free wavelength-modulation spectroscopy based on a swiftly determined wavelength-modulation frequency response function of a DFB laser. Optics Express, 2016, 24, 1723.	3.4	24
178	Assessing the impact of an alternative biochemical failure definition on radiation dose response for high-risk prostate cancer treated with external beam radiotherapy. International Journal of Radiation Oncology Biology Physics, 2005, 61, 14-19.	0.8	23
179	Modulation cancellation method for measurements of small temperature differences in a gas. Optics Letters, 2011, 36, 460.	3.3	23
180	Modulation cancellation method for isotope ^180/^160 ratio measurements in water. Optics Express, 2012, 20, 3401.	3.4	23

#	Article	IF	CITATIONS
181	Mechanisms and efficient elimination approaches of self-absorption in LIBS. Plasma Science and Technology, 2019, 21, 034016.	1.5	23
182	High-sensitivity, large dynamic range, auto-calibration methane optical sensor using a short confocal Fabry–Perot cavity. Sensors and Actuators B: Chemical, 2007, 127, 350-357.	7.8	22
183	Statistical Modeling Approach to Quantitative Analysis of Interobserver Variability in Breast Contouring. International Journal of Radiation Oncology Biology Physics, 2014, 89, 214-221.	0.8	22
184	A Super-Learner Model for Tumor Motion Prediction and Management in Radiation Therapy: Development and Feasibility Evaluation. Scientific Reports, 2019, 9, 14868.	3.3	22
185	Design and commissioning of an image-guided small animal radiation platform and quality assurance protocol for integrated proton and x-ray radiobiology research. Physics in Medicine and Biology, 2019, 64, 135013.	3.0	22
186	A pencil-beam photon dose algorithm for stereotactic radiosurgery using a miniature multileaf collimator. Medical Physics, 1998, 25, 841-850.	3.0	21
187	Anatomic distribution of [ 18 F] fluorodeoxyglucose-avid lymph nodes in patients with cervical cancer. Practical Radiation Oncology, 2013, 3, 45-53.	2.1	21
188	Automated Knowledge-Based Intensity-Modulated Proton Planning: An International Multicenter Benchmarking Study. Cancers, 2018, 10, 420.	3.7	21
189	Current State of Image Guidance in Radiation Oncology: Implications for PTV Margin Expansion and Adaptive Therapy. Seminars in Radiation Oncology, 2018, 28, 238-247.	2.2	21
190	Medical Physics, 2012, 39, 5136-5144.	3.0	20
191	Ppb-level mid-infrared ethane detection based on three measurement schemes using a 3.34-μm continuous-wave interband cascade laser. Applied Physics B: Lasers and Optics, 2016, 122, 1.	2.2	20
192	Generalized optical design of two-spherical-mirror multi-pass cells with dense multi-circle spot patterns. Applied Physics Letters, 2020, 116, .	3.3	20
193	Narrowband Perfect Absorber Based on Dielectric-Metal Metasurface for Surface-Enhanced Infrared Sensing. Applied Sciences (Switzerland), 2020, 10, 2295.	2.5	20
194	Compact quartz-enhanced photoacoustic sensor for ppb-level ambient NO2 detection by use of a high-power laser diode and a grooved tuning fork. Photoacoustics, 2022, 25, 100325.	7.8	20
195	Improving accuracy of electron density measurement in the presence of metallic implants using orthovoltage computed tomography. Medical Physics, 2008, 35, 1932-1941.	3.0	19
196	Metabolic Imaging Biomarkers of Postradiotherapy Xerostomia. International Journal of Radiation Oncology Biology Physics, 2012, 83, 1609-1616.	0.8	19
197	Perturbation of waterâ€equivalent thickness as a surrogate for respiratory motion in proton therapy. Journal of Applied Clinical Medical Physics, 2016, 17, 368-378.	1.9	19
198	Review of methodological and experimental LIBS techniques for coal analysis and their application in power plants in China. Frontiers of Physics, 2016, 11, 1.	5.0	19

#	Article	IF	CITATIONS
199	Increase in Superficial Dose in Whole-Breast Irradiation With Halcyon Straight-Through Linac Compared With Traditional C-arm Linac With Flattening Filter: InÁvivo Dosimetry and Planning Study. Advances in Radiation Oncology, 2020, 5, 120-126.	1.2	18
200	A sensitivity-guided algorithm for automated determination of IMRT objective function parameters. Medical Physics, 2006, 33, 2935-2944.	3.0	17
201	A serial 4DCT study to quantify range variations in charged particle radiotherapy of thoracic cancers. Journal of Radiation Research, 2014, 55, 309-319.	1.6	17
202	Development of Ultra-High Dose-Rate (FLASH) Particle Therapy. IEEE Transactions on Radiation and Plasma Medical Sciences, 2022, 6, 252-262.	3.7	17
203	Compact portable QEPAS multi-gas sensor. Proceedings of SPIE, 2011, , .	0.8	16
204	Investigation on spatial distribution of optically thin condition in laser-induced aluminum plasma and its relationship with temporal evolution of plasma characteristics. Journal of Analytical Atomic Spectrometry, 2017, 32, 1519-1526.	3.0	16
205	Ppbv-Level Ethane Detection Using Quartz-Enhanced Photoacoustic Spectroscopy with a Continuous-Wave, Room Temperature Interband Cascade Laser. Sensors, 2018, 18, 723.	3.8	16
206	Multiple-sound-source-excitation quartz-enhanced photoacoustic spectroscopy based on a single-line spot pattern multi-pass cell. Applied Physics Letters, 2021, 118, .	3.3	16
207	Dosimetric verification for intensity-modulated radiotherapy of thoracic cancers using experimental and Monte Carlo approaches. International Journal of Radiation Oncology Biology Physics, 2006, 66, 939-948.	0.8	15
208	IGRT has limited clinical value due to lack of accurate tumor delineation. Medical Physics, 2013, 40, 040601.	3.0	15
209	Cavity-enhanced photoacoustic sensor based on a whispering-gallery-mode diode laser. Atmospheric Measurement Techniques, 2019, 12, 1905-1911.	3.1	15
210	A novel patch-field design using an optimized grid filter for passively scattered proton beams. Physics in Medicine and Biology, 2007, 52, N265-N275.	3.0	14
211	The precision of respiratory-gated delivery of synchrotron-based pulsed beam proton therapy. Physics in Medicine and Biology, 2010, 55, 7633-7647.	3.0	14
212	Fast range-corrected proton dose approximation method using prior dose distribution. Physics in Medicine and Biology, 2012, 57, 3555-3569.	3.0	14
213	Continuous-wave cavity ringdown spectroscopy based on the control of cavity reflection. Optics Express, 2013, 21, 17961.	3.4	14
214	Learning anatomy changes from patient populations to create artificial CT images for voxelâ€ <del>l</del> evel validation of deformable image registration. Journal of Applied Clinical Medical Physics, 2016, 17, 246-258.	1.9	14
215	Influence of intravenous contrast agent on dose calculation in proton therapy using dual energy CT. Physics in Medicine and Biology, 2019, 64, 125024.	3.0	14
216	Improving Soft-Tissue Contrast in Four-Dimensional Computed Tomography Images of Liver Cancer Patients Using a Deformable Image Registration Method. International Journal of Radiation Oncology Biology Physics, 2008, 72, 201-209.	0.8	13

#	Article	IF	CITATIONS
217	Predictive Value of 18F-Fluorodeoxyglucose Uptake by Positron Emission Tomography for Non-Small Cell Lung Cancer Patients Treated with Radical Radiotherapy. Journal of Radiation Research, 2010, 51, 465-471.	1.6	13
218	A statistical modeling approach for evaluating auto-segmentation methods for image-guided radiotherapy. Computerized Medical Imaging and Graphics, 2012, 36, 492-500.	5.8	13
219	A novel doseâ€based positioning method for CT imageâ€guided proton therapy. Medical Physics, 2013, 40, 051714.	3.0	13
220	Development of a Laboratory Cement Quality Analysis Apparatus Based on Laser-Induced Breakdown Spectroscopy. Plasma Science and Technology, 2015, 17, 897-903.	1.5	13
221	Parameters Optimization of Laser-Induced Breakdown Spectroscopy Experimental Setup for the Case with Beam Expander. Plasma Science and Technology, 2015, 17, 914-918.	1.5	13
222	Robust optimization for intensityâ€modulated proton therapy with soft spot sensitivity regularization. Medical Physics, 2019, 46, 1408-1425.	3.0	13
223	Investigation and cancellation of residual amplitude modulation in fiber electro-optic modulator based frequency modulation gas sensing technique. Sensors and Actuators B: Chemical, 2014, 196, 23-30.	7.8	12
224	Intensity-Stabilized Fast-Scanned Direct Absorption Spectroscopy Instrumentation Based on a Distributed Feedback Laser with Detection Sensitivity down to 4 × 10â^6. Sensors, 2016, 16, 1544.	3.8	12
225	Quartz-Enhanced Photothermal-Acoustic Spectroscopy for Trace Gas Analysis. Applied Sciences (Switzerland), 2019, 9, 4021.	2.5	12
226	Laser induced thermoelastic contributions from windows to signal background in a photoacoustic cell. Photoacoustics, 2021, 22, 100257.	7.8	12
227	Piezo-enhanced acoustic detection module for mid-infrared trace gas sensing using a grooved quartz tuning fork. Optics Express, 2019, 27, 35267.	3.4	12
228	The delivery of IMRT with a single physical modulator for multiple fields: a feasibility study for paranasal sinus cancer. International Journal of Radiation Oncology Biology Physics, 2004, 58, 876-887.	0.8	11
229	Use of fractional dose–volume histograms to model risk of acute rectal toxicity among patients treated on RTOG 94-06. Radiotherapy and Oncology, 2012, 104, 109-113.	0.6	11
230	Anisotropic Margin Expansions in 6 Anatomic Directions for Oropharyngeal Image Guided Radiation Therapy. International Journal of Radiation Oncology Biology Physics, 2013, 87, 596-601.	0.8	11
231	Multi-Quartz Enhanced Photoacoustic Spectroscopy with Different Acoustic Microresonator Configurations. Journal of Spectroscopy, 2015, 2015, 1-6.	1.3	11
232	Characterization of the Megavoltage Cone-Beam Computed Tomography (MV-CBCT) System on HalcyonTM for IGRT: Image Quality Benchmark, Clinical Performance, and Organ Doses. Frontiers in Oncology, 2019, 9, 496.	2.8	11
233	Ultra-repeatability measurement of the coal calorific value by XRF assisted LIBS. Journal of Analytical Atomic Spectrometry, 2020, 35, 2928-2934.	3.0	11
234	A novel methodology to directly pre-determine the relative wavelength response of DFB laser in wavelength modulation spectroscopy. Optics Express, 2019, 27, 1249.	3.4	11

#	Article	IF	CITATIONS
235	A CT-based software tool for evaluating compensator quality in passively scattered proton therapy. Physics in Medicine and Biology, 2010, 55, 6759-6771.	3.0	10
236	MRI-Based Computed Tomography Metal Artifact Correction Method for Improving Proton Range Calculation Accuracy. International Journal of Radiation Oncology Biology Physics, 2015, 91, 849-856.	0.8	10
237	Automated rapid blood culture sensor system based on diode laser wavelength-modulation spectroscopy for microbial growth analysis. Sensors and Actuators B: Chemical, 2018, 273, 656-663.	7.8	10
238	Acoustic Detection Module Design of a Quartz-Enhanced Photoacoustic Sensor. Sensors, 2019, 19, 1093.	3.8	10
239	Impact of fractionation and number of fields on dose homogeneity for intra-fractionally moving lung tumors using scanned carbon ion treatment. Radiotherapy and Oncology, 2016, 118, 498-503.	0.6	9
240	Species distribution in laser-induced plasma on the surface of binary immiscible alloy. Spectrochimica Acta, Part B: Atomic Spectroscopy, 2019, 158, 105644.	2.9	9
241	Simultaneous multi-gas detection between 3 and 4 μm based on a 2.5-m multipass cell and a tunable Fabry-Pérot filter detector. Spectrochimica Acta - Part A: Molecular and Biomolecular Spectroscopy, 2019, 216, 154-160.	3.9	9
242	Concentric multipass cell enhanced double-pulse laser-induced breakdown spectroscopy for sensitive elemental analysis. Spectrochimica Acta, Part B: Atomic Spectroscopy, 2020, 168, 105851.	2.9	9
243	Elliptical-tube off-beam quartz-enhanced photoacoustic spectroscopy. Applied Physics Letters, 2022, 120, .	3.3	9
244	Real time detection of exhaled human breath using quantum cascade laser based sensor technology. , 2012, , .		8
245	Quartz-enhanced conductance spectroscopy for nanomechanical analysis of polymer wire. Applied Physics Letters, 2015, 107, 221903.	3.3	8
246	Digital reconstruction of high-quality daily 4D cone-beam CT images using prior knowledge of anatomy and respiratory motion. Computerized Medical Imaging and Graphics, 2015, 40, 30-38.	5.8	7
247	Near-Infrared Quartz-Enhanced Photoacoustic Sensor for H2S Detection in Biogas. Applied Sciences (Switzerland), 2019, 9, 5347.	2.5	7
248	Evaluation of Two-Voltage and Three-Voltage Linear Methods for Deriving Ion Recombination Correction Factors in Proton FLASH Irradiation. IEEE Transactions on Radiation and Plasma Medical Sciences, 2022, 6, 263-270.	3.7	7
249	A Volumetric Trend Analysis of the Prostate and Seminal Vesicles During a Course of Intensity-Modulated Radiation Therapy. American Journal of Clinical Oncology: Cancer Clinical Trials, 2010, 33, 173-175.	1.3	7
250	Optimization Investigations of Continuous Wave Cavity Ringdown Spectroscopy. Applied Physics Express, 2013, 6, 072402.	2.4	6
251	Evaluation and Application of U.S. Medical Proton Facilities for Single Event Effects Test. IEEE Transactions on Nuclear Science, 2015, 62, 2490-2497.	2.0	6
252	Preliminary Radiation Testing of a State-of-the-Art Commercial 14nm CMOS Processor /		6

System-on-a-Chip., 2015, , .

#	Article	IF	CITATIONS
253	Stability Enhanced Online Powdery Cement Raw Materials Quality Monitoring Using Laser-Induced Breakdown Spectroscopy. IEEE Photonics Journal, 2017, 9, 1-10.	2.0	6
254	Laser-induced plasma characterization through self-absorption quantification. Journal of Quantitative Spectroscopy and Radiative Transfer, 2018, 213, 143-148.	2.3	6
255	Daily targeting of liver tumors: Screening patients with a mock treatment and using a combination of 2007, 34, 4591-4593.	3.0	5
256	Predicting oropharyngeal tumor volume throughout the course of radiation therapy from pretreatment computed tomography data using general linear models. Medical Physics, 2014, 41, 051705.	3.0	5
257	Optical Detection Technique Using Quartz-Enhanced Photoacoustic Spectrum. International Journal of Thermophysics, 2015, 36, 1297-1304.	2.1	5
258	Cherenkov imaging for Total Skin Electron Therapy (TSET). , 2018, , .		5
259	Position effect of laser beam waist in quartz-enhanced photoacoustic spectroscopy. Infrared Physics and Technology, 2022, 125, 104271.	2.9	5
260	Automating RTOG-defined target volumes for postmastectomy radiation therapy. Practical Radiation Oncology, 2011, 1, 97-104.	2.1	4
261	Improved human observer performance in digital reconstructed radiograph verification in head and neck cancer radiotherapy. International Journal of Computer Assisted Radiology and Surgery, 2015, 10, 1667-1673.	2.8	4
262	Accurate quantitative CF-LIBS analysis of both major and minor elements in alloys via iterative correction of plasma temperature and spectral intensity. Plasma Science and Technology, 2018, 20, 035502.	1.5	4
263	Initial Clinical Experience Treating Patients With Gynecologic Cancers on a 6MV Flattening Filter Free O-Ring Linear Accelerator. Advances in Radiation Oncology, 2020, 5, 920-928.	1.2	4
264	Daily Bone Alignment With Limited Repeat CT Correction Rivals Daily Ultrasound Alignment for Prostate Radiotherapy. International Journal of Radiation Oncology Biology Physics, 2008, 71, 274-280.	0.8	3
265	Proton therapy for Hodgkin lymphoma: does a case report make the case?. Leukemia and Lymphoma, 2010, 51, 1397-1398.	1.3	3
266	Compact sound-speed sensor for quartz enhanced photoacoustic spectroscopy based applications. Review of Scientific Instruments, 2015, 86, 044903.	1.3	3
267	A compact mid-infrared dual-gas CH <sub>4</sub> /C <sub>2</sub> H <sub>6</sub> sensor using a single interband cascade laser and custom electronics. Proceedings of SPIE, 2017, , .	0.8	3
268	High-efficiency frequency upconversion of 1.5Âμm laser based on a doubly resonant external ring cavity with a low finesse for signal field. Applied Physics B: Lasers and Optics, 2017, 123, 1.	2.2	3
269	Influence of Tuning Fork Resonance Properties on Quartz-Enhanced Photoacoustic Spectroscopy Performance. Sensors, 2019, 19, 3825.	3.8	3
270	Quartz Enhanced Conductance Spectroscopy for Polymer Nano-Mechanical Thermal Analysis. Applied Sciences (Switzerland), 2020, 10, 4954.	2.5	3

#	Article	IF	CITATIONS
271	Quartz Enhanced Photoacoustic Detection Based on an Elliptical Laser Beam. Applied Sciences (Switzerland), 2020, 10, 1197.	2.5	3
272	Numerical simulation of laser-induced plasma in background gas considering multiple interaction processes. Plasma Science and Technology, 2021, 23, 035001.	1.5	3
273	Quartz-enhanced photoacoustic spectroscopy exploiting a fast and wideband electro-mechanical light modulator. Optics Express, 2020, 28, 27966.	3.4	3
274	Forecasting longitudinal changes in oropharyngeal tumor morphology throughout the course of head and neck radiation therapy. Medical Physics, 2014, 41, 081708.	3.0	2
275	Innovative quartz enhanced photoacoustic sensors for trace gas detection. , 2016, , .		2
276	Compact, low power consumption methane sensor based on a novel miniature multipass gas cell and a CW, room temperature interband cascade laser emitting at 3.3 μm. Proceedings of SPIE, 2016, , .	0.8	2
277	New Developments in Quartz-Enhanced Photoacoustic Sensing Real-World Applications. , 2020, , .		2
278	Species distribution in laser-induced plasma on the surface of binary miscible alloy. Spectrochimica Acta, Part B: Atomic Spectroscopy, 2020, 173, 105987.	2.9	2
279	Recent advances in quartz-enhanced photoacoustic sensing. , 2018, , .		2
280	Improvements in medical CT image reconstruction accuracy in the presence of metal objects by using x-rays up to 1 MeV. Proceedings of SPIE, 2009, , .	0.8	1
281	Anatomic variation and dosimetric consequences of neoadjuvant hormone therapy before radiation therapy for prostate cancer. Practical Radiation Oncology, 2013, 3, 329-336.	2.1	1
282	How Fast Does Real-Time Delivery Affirmation Need To Be?. International Journal of Radiation Oncology Biology Physics, 2014, 89, 623-625.	0.8	1
283	Design and Optimization of QTF Chopper for Quartz-Enhanced Photoacoustic Spectroscopy. International Journal of Thermophysics, 2015, 36, 1289-1296.	2.1	1
284	Homogeneous-material-based calibration method for correcting laser-induced breakdown spectroscopy measurement-error bias in the case of dust pollution. Applied Optics, 2017, 56, 9644.	1.8	1
285	Efficient double-scattering proton therapy with a patient-specific bolus. Physica Medica, 2018, 50, 1-6.	0.7	1
286	Compact TDLAS Based Sensors Using Interband Cascade Lasers for CH_2O and CH_4 Trace Gas Measurements. , 2015, , .		1
287	Investigation and performance evaluation of optically thin laser-induced breakdown spectroscopy without self-absorption. Scientia Sinica: Physica, Mechanica Et Astronomica, 2017, 47, 124201.	0.4	1
288	Quantitative CF-LIBS analysis of alloys via comprehensive calibration of plasma temperature and spectral intensity. Scientia Sinica: Physica, Mechanica Et Astronomica, 2018, 48, 014201.	0.4	1

#	Article	IF	CITATIONS
289	Novel direct conversion imaging detector without selenium or semiconductor conversion layer. , 2019, , .		1
290	Mid-infrared detection of atmospheric CH4, N2O and H2O based on a single continuous wave quantum cascade laser. , 2015, , .		0
291	Single-tube on beam quartz-enhanced photoacoustic spectrophones exploiting a custom quartz tuning fork operating in the overtone mode. Proceedings of SPIE, 2017, , .	0.8	Ο
292	Recent advances in quartz-enhanced photoacoustic sensors employing custom tuning fork operating at the first overtone flexural mode. , 2017, , .		0
293	Technical Note: Solving the "Chinese postman problem―for effective contour deformation. Medical Physics, 2018, 45, 767-772.	3.0	0
294	Quartz-enhanced photoacoustic spectroscopy for CO detection in SF6 decomposition. , 2021, , .		0
295	Quartz tuning forks employed as photodetectors in TDLAS sensors. , 2021, , .		Ο
296	SU-E-J-138: The Effect of Shoulder Variation on IMRT and SmartArc Plans for Head and Neck Cancer. Medical Physics, 2011, 38, 3474-3474.	3.0	0
297	Recent advances of mid–infrared compact, field deployable sensors and their real world applications in the petrochemical industry, atmospheric chemistry and security. , 2016, , .		Ο
298	Near-infrared Quartz Enhanced Photoacoustic Sensor for Sub-ppm Level H2S Detection based on a Fiber-amplifier Source. , 2016, , .		0
299	Monitoring of atmospheric Methane and Ethane using two Continuous-Wave Interband Cascade Lasers. , 2016, , .		Ο
300	Micro-resonator Parameter Optimization of a QEPAS Spectrophone using a Custom Quartz Tuning Fork with large Prong Spacing. , 2016, , .		0
301	Mid-IR laser-based sensor for hydrogen peroxide detection. SPIE Newsroom, 0, , .	0.1	Ο
302	Nitrogen Dioxide Detection by use of Photoacoustic Spectroscopy with a High Power Violet-Blue Diode Laser. , 2017, , .		0
303	Photoacoustic H2S Gas Sensor for SF6 Decomposition Analysis in an Electric Power System. , 2018, , .		Ο
304	Fast and calibration-free trace-gas monitoring based on beat frequency quartz-enhanced photoacoustic spectroscopy. , 2018, , .		0
305	N2-cooled THz quartz-enhanced photoacoustic sensor operating in pulsed mode for hydrogen sulfide detection in the part-per-billion concentration range. , 2020, , .		0
306	Advanced Topics in Particle Radiotherapy. IEEE Transactions on Radiation and Plasma Medical Sciences, 2022, 6, 247-251.	3.7	0